Journal of Geophysical Research: Planets

Supporting Information for

From lake to river: Documenting an environmental transition across the Jura/Knockfarril Hill members boundary in the Glen Torridon region of Gale crater (Mars).

G. Caravaca[1,2*], N. Mangold[2], E. Dehouck[3], J. Schieber[4], L. Zaugg[2], A.B. Bryk[5], C.M. Fedo[6], S. Le Mouélic[2], L. Le Deit[2], S.G. Banham[7], S. Gupta[7], A. Cousin[1], W. Rapin[1], O. Gasnault[1], F. Rivera-Hernández[8], R.C. Wiens[9], N.L. Lanza[10].

[1] UMR 5277 CNRS, UPS, CNES Institut de Recherche en Astrophysique et Planétologie, Université Paul Sabatier Toulouse III, Toulouse, France
[2] UMR 6112 CNRS Laboratoire de Planétologie et Géodynamique, Université de Nantes, Université d'Angers, Nantes, France.
[3] UMR 5276 Laboratoire de Géologie de Lyon—Terre Planète Environnement, Université Claude Bernard Lyon, ENS Lyon, UJM, CNRS, Villeurbanne, France
[4] Department of Geological Sciences, Indiana University, Bloomington, IN, USA
[5] University of California, Berkeley, CA, USA
[6] Department of Earth & Planetary Sciences, University of Tennessee, Knoxville, TN, USA
[7] Department of Earth Sciences and Engineering, Imperial College London, London, UK
[8] Department of Earth and Atmospheric Sciences, Georgia Institute of Technology, Atlanta, GA, USA
[9] Earth, Atmospheric, and Planetary Sciences, Purdue University, West Lafayette, IN, USA
[10] Los Alamos National Laboratory, Los Alamos, NM, USA

Contents of this file

Additional Supporting Information (Files uploaded separately)

Captions for Tables S1 to S3 (larger than 1 page, upload as separate files (also available as online data on Zenodo, cf. Caravaca *et al.*, 2022)

Introduction

This supporting information gives additional details on Earth-based example of polygonally-cracked mudstone linked to thermal cycling rather than desiccation at the time of the deposition.
This material also provides illustrations for the photogrammetric micro-DOM of the target Beauly, and line-drawing of possible channelized bodies in western part of the Antonine Wall outcrop.
Finally, tables containing the complete list of individual MAHLI and ChemCam targets investigated, detailed laminae measurements and complete ChemCam compositional data are also provided as separate files.

Addendum on the origin of polygonal cracks

Looking at the grain size of polygon layers with MAHLI (Fig. S3a) suggests that they likely are coarse mudstones (aka siltstones) following the nomenclature of Lazar *et al.* (2015). Because of framework grain support, siltstones do not contract upon drying and thus are unlikely to form desiccation cracks.
Although the literature on the formation of polygonal cracks during outcrop weathering mainly reports on this phenomenon for sandstones and granites (Williams & Robinson, 1989), it is also common in outcrop weathering of shales and mudstones. Figures S3b to S3d show polygon formation in large blocks of New Albany Shale from Kentucky, USA. These dark shales are marine in origin (no primary desiccation cracks), are not affected by moisture related shrinkage and swelling, and preferentially show development of polygonal fracture patterns in quarry operations on the exposed surface of large blocks. The patterns form preferentially in summer-fall when day-night surface temperatures of these blocks cycle by as much as 50 degrees Celsius. The thermal expansion coefficients for shales are similar to those of granite and sandstone and a 1 m block would expand-contract by several tenths of a mm under those conditions (Robertson, 1988 – USGS Open File Report 88-441).
Collectively, the observations made on the Woodland Bay cracked layers are consistent with and of the same scale and characteristics as polygonal networks observed during outcrop weathering of mudstones on Earth, the like of that are illustrated in Fig. S3.

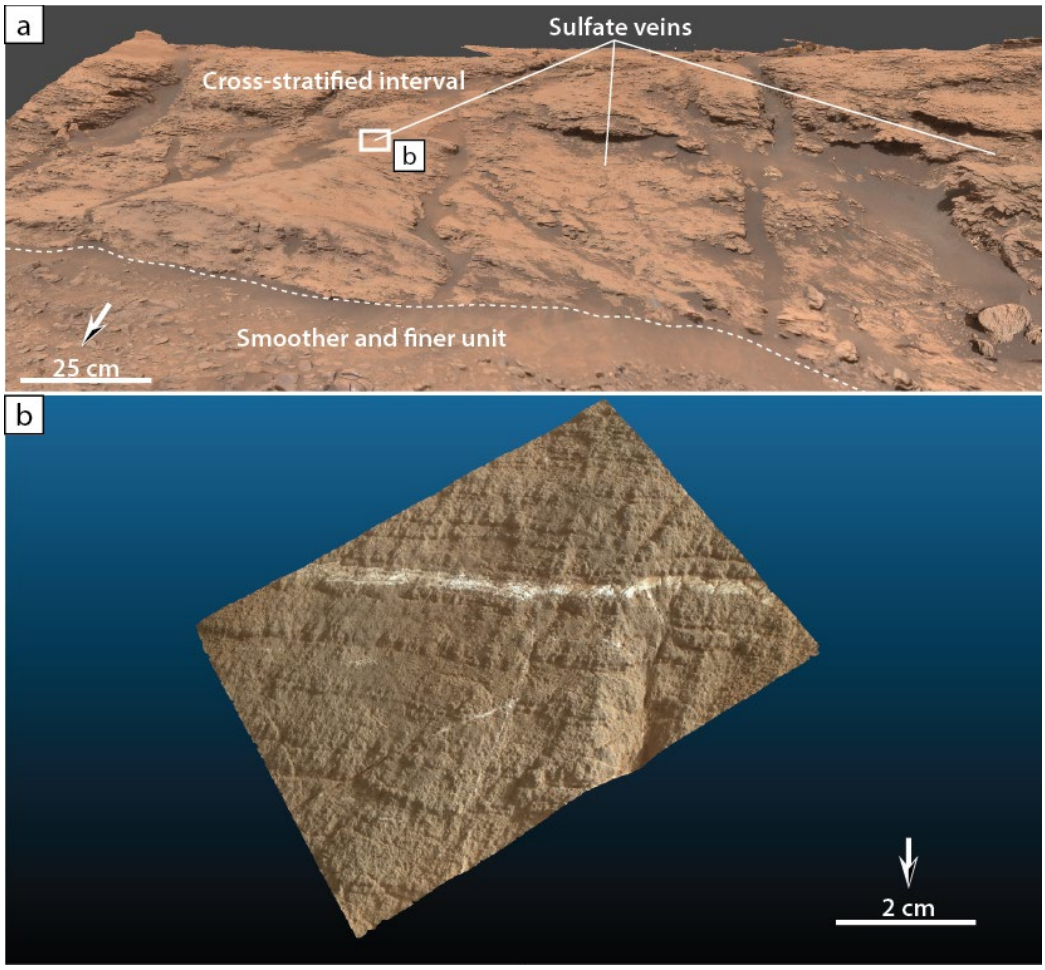

Figure S1. Detailed view of the eastern part of the Teal ridge outcrop on the DOM (see Figs. 5 and 6 of the main article). The dashed line indicates the position of the inferred sharp contact between finer and smother terrain and the coarser cross-stratified sandstones making the mesa. b) View of the µDOM of the Beauly target, computed from 20 MAHLI images taken on Sol 2443; mesh visible on Sketchfab at: https://skfb.ly/opKqs.

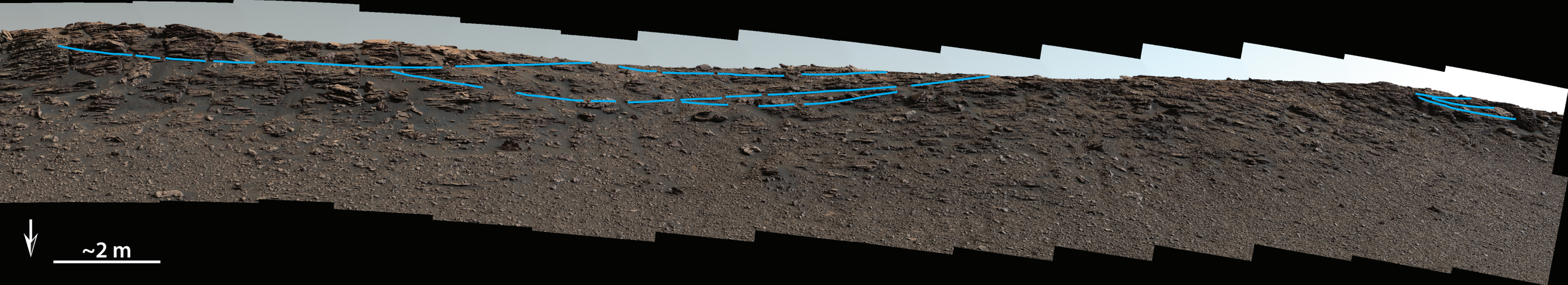
~2 m

Figure S2. (previous page) Western view of Antonine Wall outcrop in the Visionarium. Mastcam mosaic acquired on Sol 2471 (sequence mcam013112). The mosaic shows a continuous exposure of cross-stratified sandstones, exhibiting several possible meter-scale channelized bodies with concave bases (blue lines)

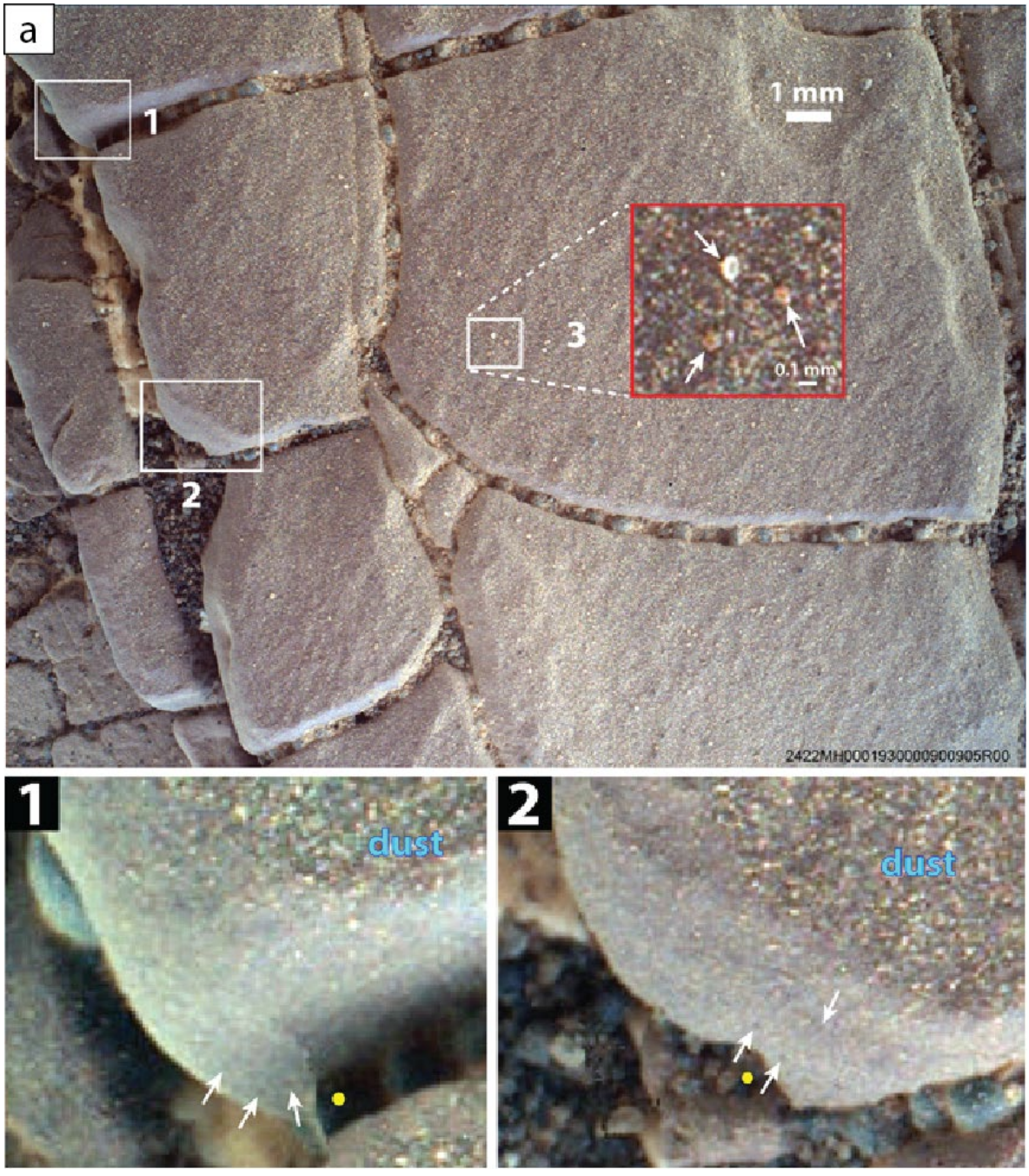

Figure S3. Likely grain size of polygon layers in Fig. 9c of the main text. Top image is a MAHLI close-up with a resolution of 17.3 microns per pixel. Numbers 1, 2, and 3 mark enlarged regions of interest. The surface of the polygons is covered with windblown material, which contains fine sand size particles (region 3 enlargement, arrows) but is dominated by finer dust. Regions 1 and

2 are comparatively dust free areas that are shown enlarged and contrast enhanced (bottom row). Arrows point to objects that are 3 pixels across and considered sediment grains (coarse silt).

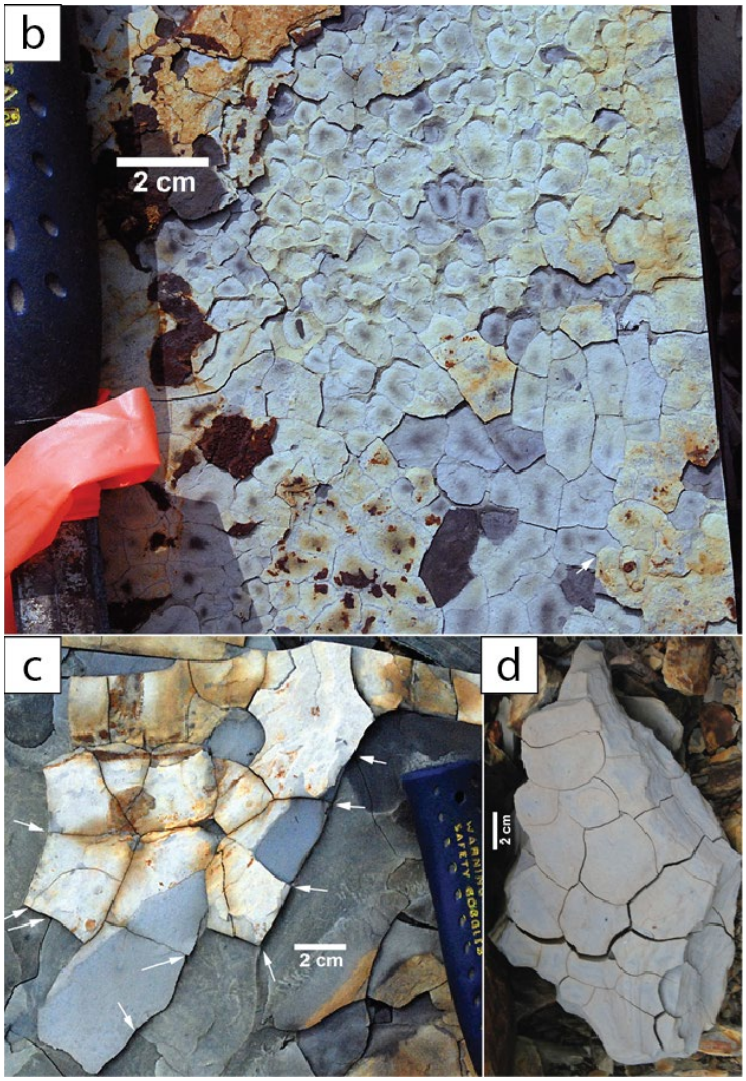

Figure S3 (cont.). Formation of cm-scale polygon networks on blocks of New Albany Shale. Although the cracks may penetrate several mm-thick shale layers, in many instances the expansion-contraction also leads to propagation of layer-parallel cracks that prevent the polygon cracks from downward propagation. As a consequence, the crack networks of successive layers generally do not match. The network mismatch is marked with white arrows in b) and c). d) In blocks of more uniform composition layer-parallel cracks are not as well developed and polygon cracks propagate across multiple layers.

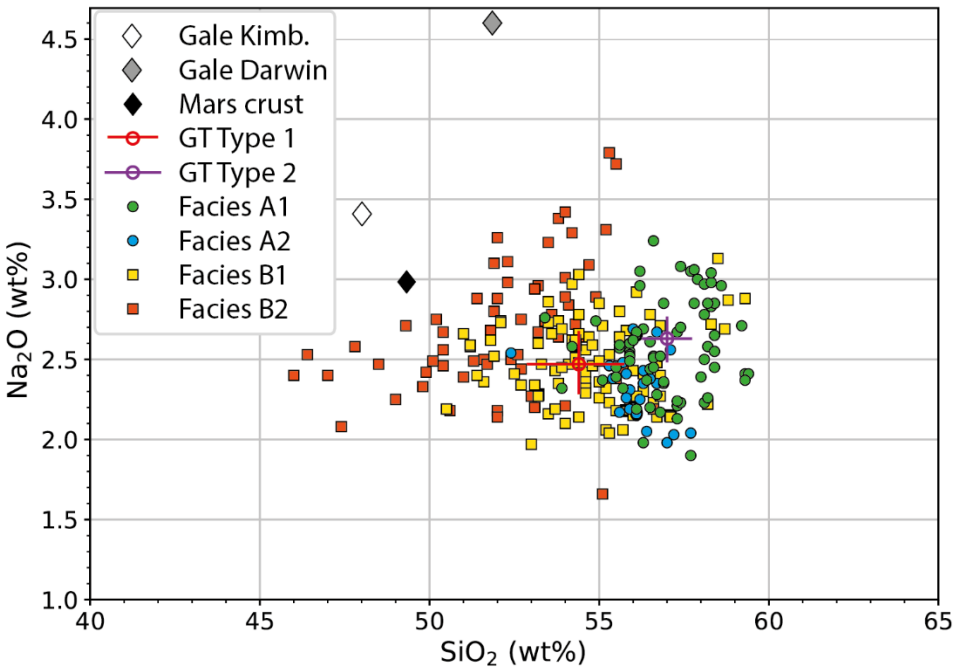

Figure S4. Major-oxide composition of GT samples in $Na_2O$and SiO_2 elements (in wt.%) as a function of the sedimentary (sub-)facies A1, A2, B1 and B2. Average Martian crust values from Taylor (2009); average Gale basin crust values from Mangold *et al.*, (2016) (Kimb.: Kimberley).

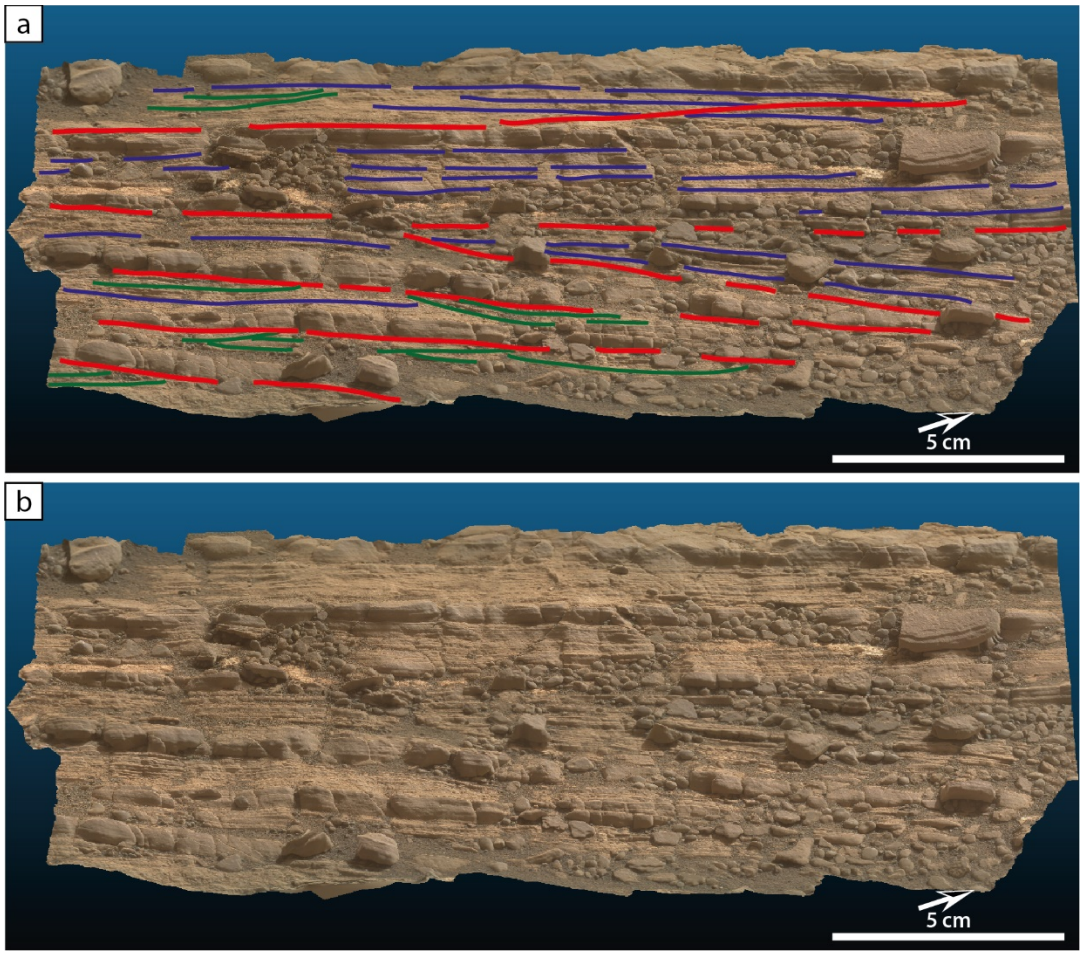

Figure S5. a) Interpreted view of the Morningside target (cf. Fig. 3b). b) Same view without interpretation.

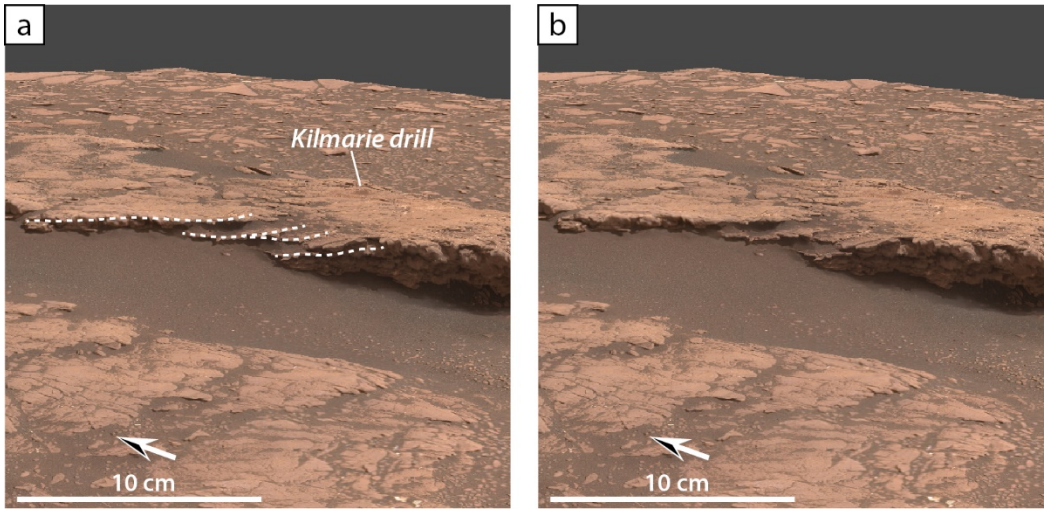

Figure S6. a) Interpreted view of the Kilmarie slab (cf. Fig. 4c). b) Same view without interpretation.

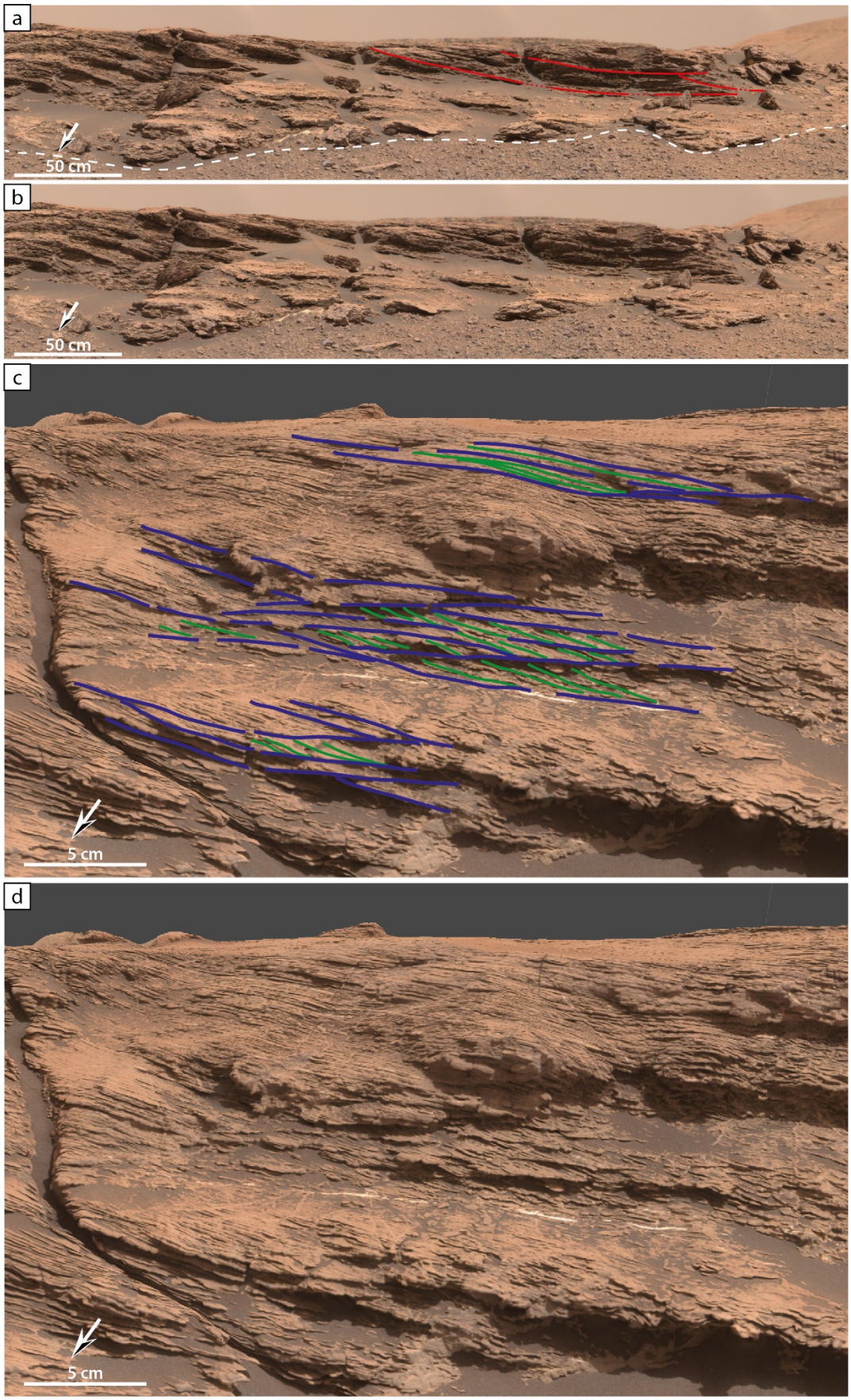
a
50 cm
b
50 cm
c
5 cm
d
5 cm

Figure S7. **(previous page)** a) Interpreted view of the western side of the Teal ridge outcrop (cf. Fig. 5b). b) Same view without interpretation. c) Interpreted view of the central part of the Teal ridge outcrop DOM (cf. Fig. 5d). d) Same view without interpretation.

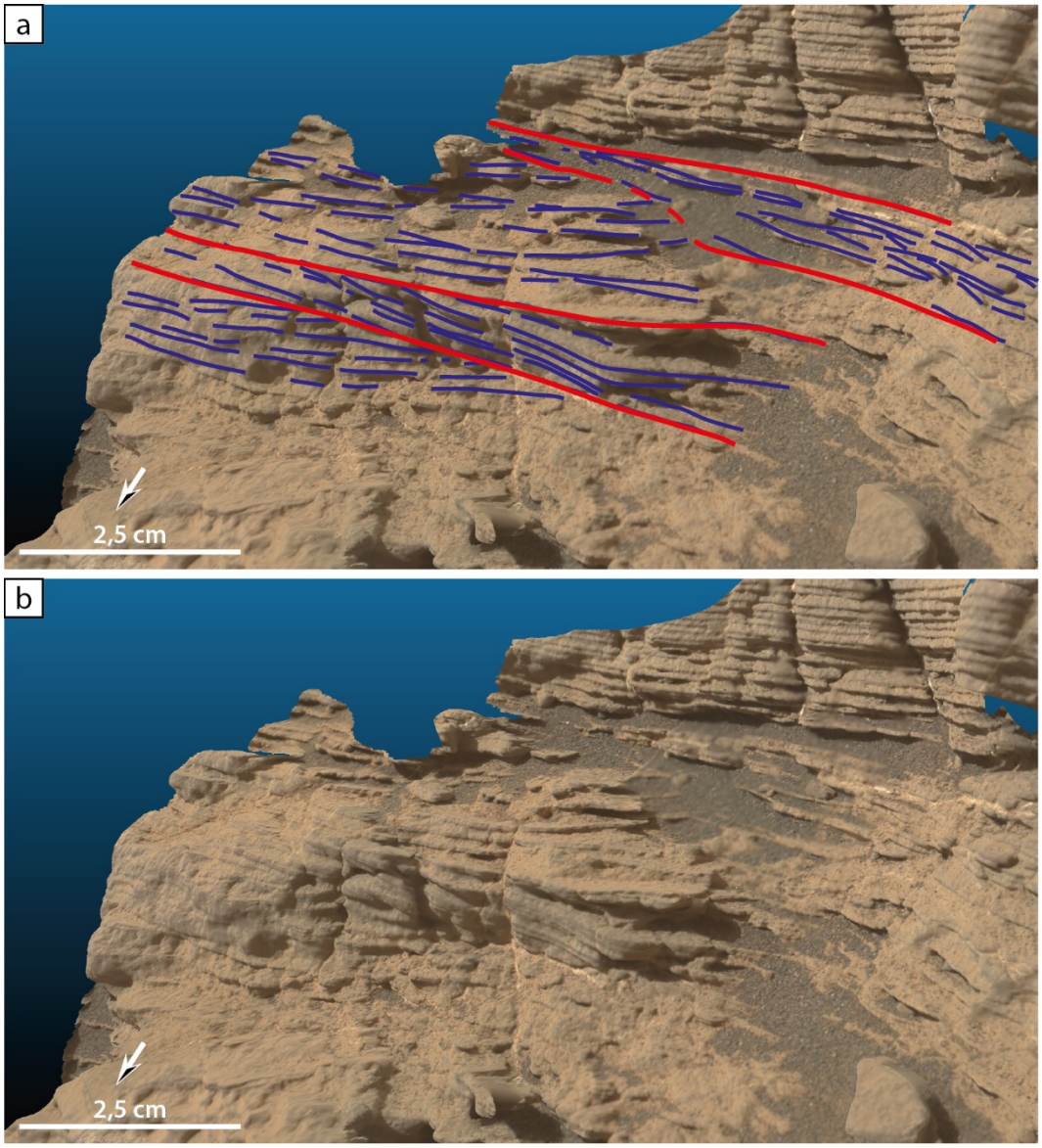

Figure S8. a) Interpreted view of the Stack_Of_Glencoul target (cf. Fig. 6c). b) Same view without interpretation.

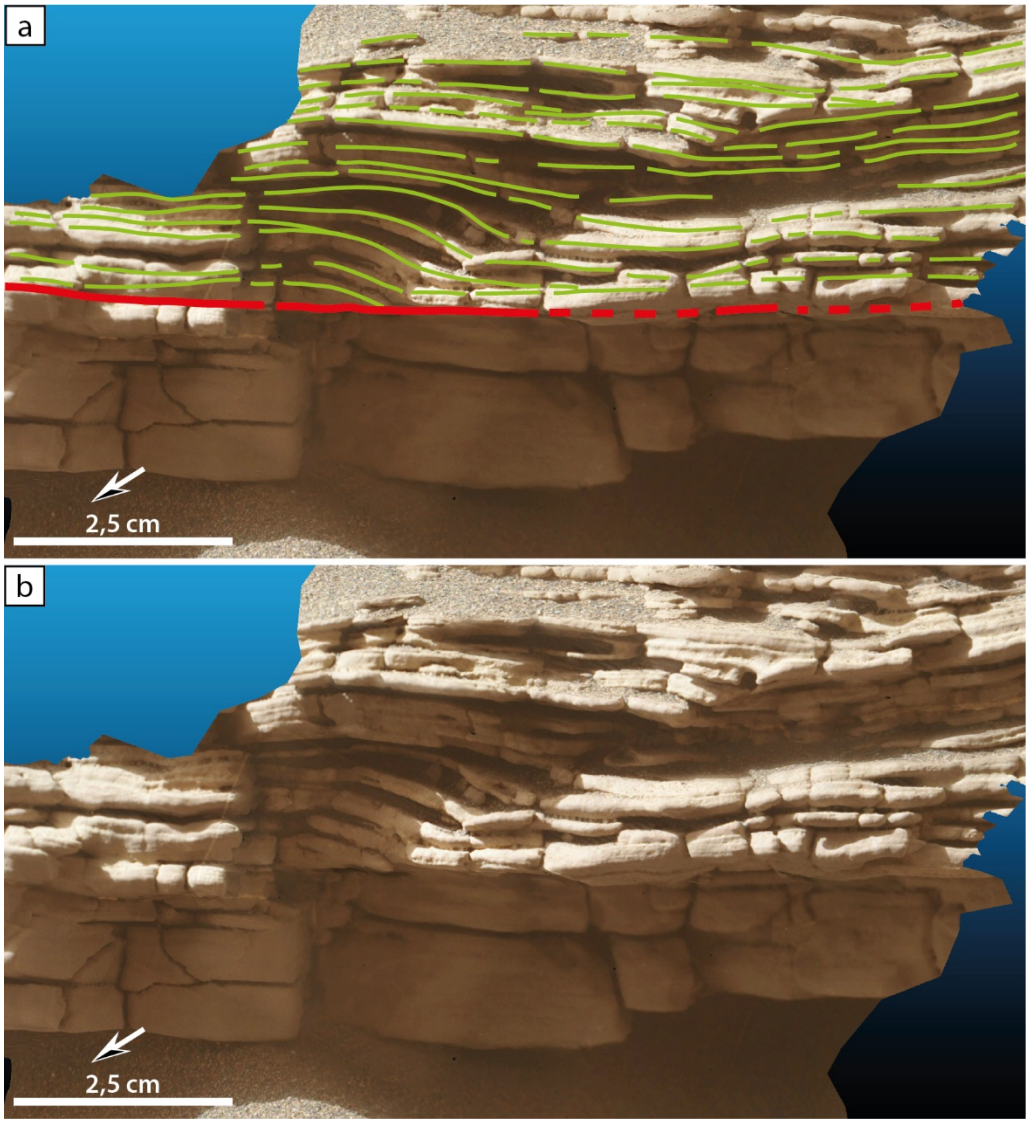

Figure S9. a) Interpreted view of the Strathdon target (cf. Fig. 7c). b) Same view without interpretation.

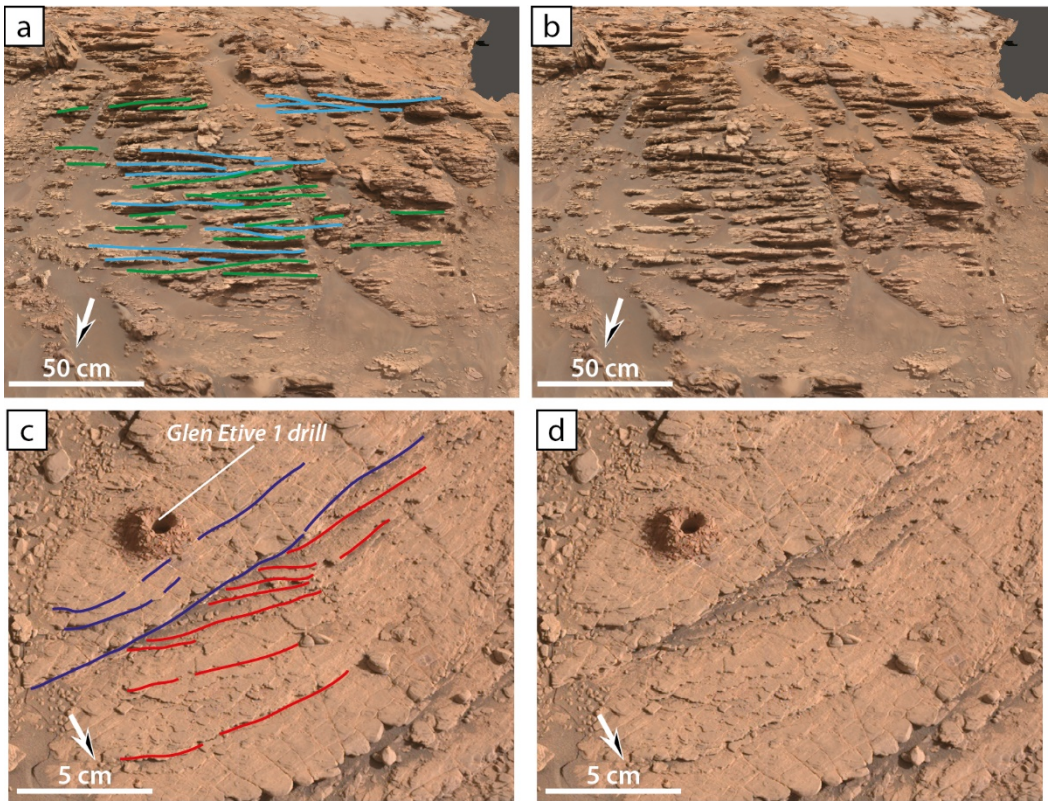

Figure S10. a) Interpreted view of the central part of the Antonine Wall cliff-face (Glen Etive outcrop) DOM target (cf. Fig. 8c). b) Same view without interpretation. c) Interpreted view of the Glen Etive 1 drill site (cf. Fig. 8d). d) Same view without interpretation.

Table S1. Complete list of individual ChemCam and MAHLI targets investigated for their grain-size, texture, and micro-structures. ChemCam targets were also investigated geochemically for Major Oxide Compositions using LIBS (Also available as dataset hosted on Zenodo, see Caravaca *et al.*, 2022).

Table S2. Table of randomized individual laminae thickness measurements on several (micro-)DOMs, and calculated arithmetic mean and standard deviation for each target and/or facies for targets featuring more than one facies (Also available as dataset hosted on Zenodo, see Caravaca *et al.*, 2022).

Table S3. Complete Major Oxide Composition data for the investigated ChemCam targets, sorted by (sub-)facies (Also available as dataset hosted on Zenodo, see Caravaca *et al.*, 2022).